High-Performance MXene/Carbon Nanotube Electrochemical Actuators for Biomimetic Soft Robotic Applications

Wei Zhang, Ke Jin, Zhen Ren, Lin Li, Longfei Chang, Chengchu Zhang, Ranran Wang, Bing Li, Guan Wu, and Ying Hu**

Ionic electrochemical actuators, which convert electrical energy into mechanical energy through electrochemical-induced ion migration, show great potential in biomimetic soft robots. However, their applications are still limited due to the influence of the electrode materials and actuator performance. Here, an MXene/carbon nanotube (CNT) heterostructural electrode-based ionic actuator is developed and realizes dexterous touch manipulation mimicking humans. In this MXene/CNT heterostructure, one-dimensional CNTs are chemically interconnected into layered two-dimensional MXene nanosheets, increasing their interlayer spacing, promoting mechanical stability, and enhancing specific surface area, which facilitates the ion migration and storage as well as electrochemical actuation. Accordingly, the MXene/CNT actuator can output excellent mechanical deformation under 2.5 V voltage, including large peak-to-peak deformation (displacement 24 mm, strain 1.54%), wide frequency response (0.1–15 Hz), large force (5 mN) and good cycling stability. The actuators can be used to construct artificial fingers to achieve gentle, multi-point, variable frequency, and synergistic touching on fragile smartphone screens, including pressing a phone number to make a call and tapping an electronic drum. Especially, this finger can tap the drum at a high frequency (13 Hz), exceeding the tapping frequency that real human fingers can reach, which demonstrates its prospect in human-computer interaction.

1. Introduction

Ions play a key role in life activities, including the conduction of nerve signals and the control of muscle stretching and contraction.[1,2] Similar to mechanism of the human muscle deformation, ionic electrochemical actuators can produce mechanical deformation through the ion migration under the electrical field,[3] which has attracted great research interest from scientists and engineers. The ionic electrochemical actuator has a trilayer structure in which a polymer electrolyte layer containing mobile ions is sandwiched between electrode layers on both sides. Under the stimulation of the applied voltage, the ionic actuator generates macroscopic bending deformation due to the asymmetric volume expansion between the electrodes caused by the ion migration and accumulation, realizing the conversion from electrical energy to mechanical energy.[4] The whole actuator structure is similar to the electrochemical supercapacitor, except that the supercapacitor can't deform. Compared with various types of soft actuators, the ionic

W. Zhang, K. Jin, Z. Ren, L. Li, L. Chang, C. Zhang, Y. Hu
Anhui Province Key Lab of Aerospace Structural Parts Forming Technology and Equipment
School of Materials Science and Engineering
Hefei University of Technology
Hefei 230009, P. R. China
E-mail: huying@hfut.edu.cn

R. Wang
State Key Laboratory of High Performance Ceramics and Superfine Microstructure
Shanghai Institute of Ceramics, Chinese Academy of Science
Shanghai 200050, P. R. China
E-mail: wangranran@mail.sic.ac.cn

B. Li
College of Intelligent Systems Science and Engineering
Harbin Engineering University
Harbin 150001, P. R. China

G. Wu
National Engineering Lab for Textile Fiber Materials & Processing Technology
School of Materials Science and Engineering
Zhejiang Sci-Tech University
Hangzhou 310018, P. R. China

The ORCID identification number(s) for the author(s) of this article can be found under https://doi.org/10.1002/adfm.202408496

DOI: 10.1002/adfm.202408496

electrochemical actuator has several advantages including low working voltage, charged surface, lightweight, easy tailoring, and facile processability.[5] Therefore, they are expected to be applied in artificial muscles, biomimetic soft robots, virtual reality, and human-computer interaction systems for manipulating smart touch-screen devices such as smartphones and tablets.[6–9]

In order to meet the practical application requirement of the ionic actuators, the key is to realize the mechanical output with large deformation, fast response, and high stability in air. As the actuation mechanism of ionic actuators is based on intercalation/deintercalation of mobile ions inside the electrodes, improving the ion migration and storage capacity of the electrodes plays important roles in the development of high-performance ionic actuators, which calls for electrode materials with high properties and optimized microstructures. At present, researchers have carried out a series of research progress in material selection and electrode structural design for ionic actuators. First, carbon nanomaterials such as carbon nanotubes (CNTs) and graphene with good conductivity and large specific surface area are widely used as electrode materials to prepare ionic actuators,[10–12] and microstructural electrodes such as vertical-aligned electrodes[13,14] or three-dimensional (3D) porous network electrodes[15,16] are designed to improve the deformation displacement, response time, and cycling stability of the actuators. The doping of elements with electroactivity (e.g., nitrogen, boron, sulfur, phosphorus) in the electrode materials is regarded as another efficient way to improve the actuation performance.[17] These incorporated chemical elements provide more electrochemical active sites for electrochemical redox reactions, thus improving the capacitance and actuation performance of the actuator.[18] For example, Oh et al. prepared an ionic actuator with a 3D nanostructure electrode composed of graphitic carbon nitride and nitrogen-doped graphene, which can reach a large bending strain of 0.52%.[19] In addition, some new types of nanostructured hybrid materials, such as black phosphorus,[20] MoS_2,[21] MoS_2-graphene hybrid,[22] graphdiyne,[23] carbon/MOF (covalent-organic framework) hybrid,[24] are also explored as the electrode materials for the high-performance ionic actuators. These research results indicate that new electrode materials and structure designs are feasible to improve the performance of ionic actuators. However, the current application performance of the ionic actuators is limited, especially in biomimetic robotics and human-computer interaction. For example, it can only be used to perform simple fixed-point touch on smartphones.[6,22] Realizing dexterous biomimetic robotic touch operations (e.g., continuous, multipoint, and high-frequency touch) that are similar to or even surpass the touch operation of the real human fingers is still a challenge. Therefore, developing new types of electrode materials and structures to further improve the performance of ionic actuators is highly desirable.

The emergence of MXene has brought a new strategy for the development of ionic electrochemical actuators. Ti_3C_2Tx MXene is a new type of two-dimensional (2D) transition metal carbides and nitrides.[25,26] It has remarkable chemical and physical properties including fast charge storage capacity, high mechanical strength, excellent electrical conductivity,[27,28] abundant surface active groups (—OH, —F or —O), and electrochemical activity,[29] which is promising in energy storage and conversion fields. More importantly, as a 2D layered structured material, MXene has larger interlayer spacing (≈1.31 nm) than graphite (0.34 nm) and 1T MoS_2 (0.62 nm),[30] which makes it more prone to ion intercalation/deintercalation and rapid diffusion. Therefore, MXene is considered a promising candidate for ionic electrochemical actuators.[31] So far, there has been some pioneering research work on MXene-based ionic electrochemical actuators. Gao et al. fabricated an electrochemical actuator by using MXene (Ti_3C_2Tx) as electrode materials and gel electrolyte (PVA—H_2SO_4). The actuator produced bending deformation with strain up to 0.26% with excellent retention after 10 000 cycles.[32] Oh et al. reported an ionic actuator by assembling Ti_3C_2Tx with conductive polymer as an electrode, which exhibits a high bending strain of 1.37%.[33] However, due to the existing aggregation and restacking of MXene nanosheets caused by the van der Waals interaction and hydrogen bonding,[34,35] the accessibility to the electrolyte ions is reduced, and the diffusion and storage of ions in MXene layers are greatly affected, leading to an unsatisfactory electrochemical utilization ration.[36,37] The preparation of MXene hybrid electrode by combing additive materials such as polystyrene microspheres,[38] PEDOT:PSS and Ag nanowires,[7] methylcellulose,[39] and metal-organic framework (MOF),[40] with MXene nanosheets is regarded as an effective way to avoid this iusse. But up to now, the excellent performance of these MXene hybrid electrode-based electrochemical actuators and their applications in dexterous biomimetic touch manipulation in human-computer interaction have not been achieved, which may be influenced by the properties of the additive materials and their interaction with MXene nanosheets. Therefore, it remains crucial to design more suitable materials to adjust the interlayer structure of MXene nanosheets and improve their electrode properties, thereby enhancing the actuation performance of MXene-based ionic actuators as well as promoting their applications.

In this work, MXene/CNT heterostructure composites with adjustable interlayer spacing are fabricated and used as electrode materials for the construction of high-performance ionic electrochemical actuators, which can be used to construct artificial fingers for human-computer interaction. In this one-dimensional (1D)/2D heterostructure composite, carboxyl CNTs are chemically interconnected into MXene nanosheets through the esterification reaction, increasing the interlayer spacing of the MXene layers, alleviating restacking of MXene nanosheets, improving the mechanical stability, and enhancing the specific surface area and pore size distributions. Therefore, the MXene/CNT heterostructure composite can provide more ordered channels and storage space for the ions, which is advantageous to ion migration and storage as well as electrochemical actuation. By utilizing the MXene/CNT as the electrode with polymer and ionic liquid as a polyelectrolyte interlayer, an MXene/CNT electrode-based ionic actuator is fabricated. This MXene/CNT actuator can generate high-performance deformation under a 2.5 V voltage stimulation in air, including a large peak-to-peak bending displacement (24 mm) and strain (1.54%), a wide frequency response (0.1–15 Hz), high power density (18.44 kW m^{-3}) and energy density (7.04 kJ m^{-3}), and excellent cycle stability (10 000 cycles). It can also move a clip with a weight of 500 mg under electrical voltage stimulation, which is 15 times its own weight. Furthermore, by connecting the MXene/CNT actuator to a solar cell, bending deformation under light illumination can be also realized.

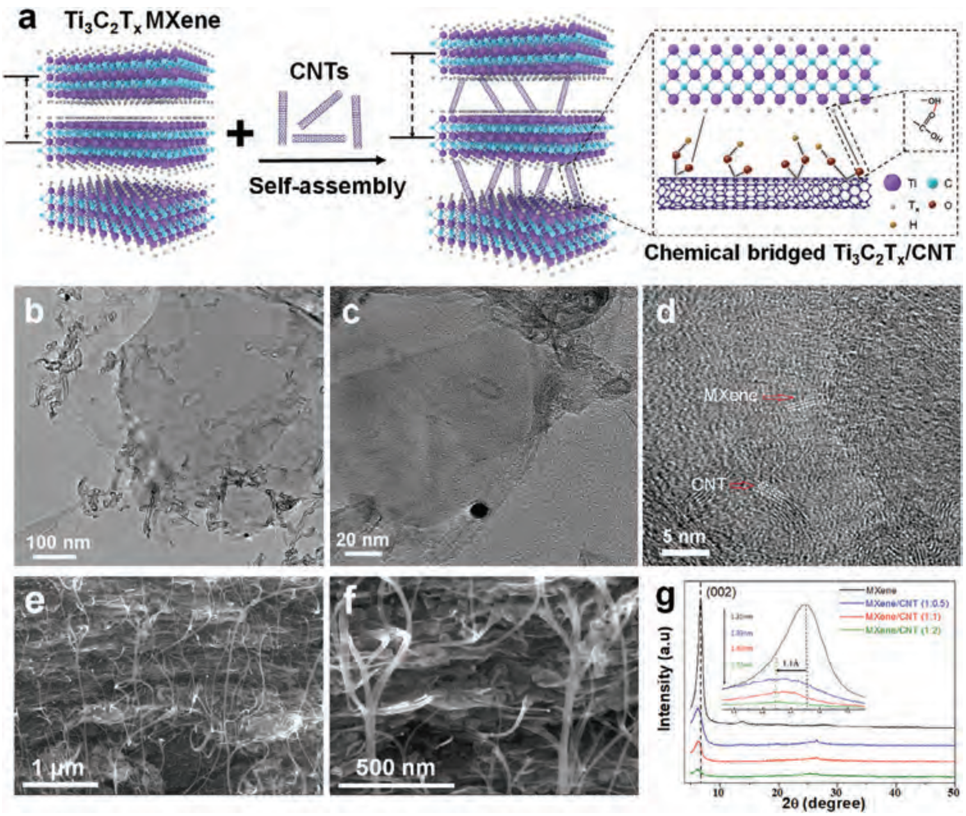

Figure 1. Fabrication and characterization of MXene/CNT heterostructure electrode. a) Schematic diagram of the microstructure of MXene/CNT electrode and atomic bond structure between MXene and carboxyl CNT. b–d) TEM images of MXene/CNT at low, middle, and high magnifications, respectively. e,f) Cross-sectional SEM images of MXene/CNT film at low and high magnifications, respectively. g) XRD patterns of the MXene and MXene/CNT with different MXene to CNT weight ratios. The inset shows the magnified XRD pattern.

Owing to the remarkable actuation performance, the actuator can be applied to the human-computer interaction field. The artificial fingers constructed from the MXene/CNT actuators can mimic human fingers to press phone numbers and make a call on a smartphone, and achieve variable-frequency synergistic sequential tapping on an electronic drum. In particular, the artificial finger can play the electronic drum with a frequency of up to 13 Hz, which exceeds the normal tapping frequency that the human fingers can reach. Besides, other biomimetic applications of the MXene/CNT actuator are also demonstrated, such as a soft mechanical claw that grasps an object, a biomimetic dragonfly flapping its wings, and artificial leaves that open under light. These results not only reveal the importance of electrode microstructure in the design of ionic actuators, but also indicate the fascinating application prospects of ionic actuators in human-computer interaction and biomimetic robotics.

2. Results and Discussion

2.1. Preparation and Structural Characterization

Figure 1a shows a schematic diagram of adjusting the interlayer spacing of the layered Ti_3C_2Tx MXene nanosheets by the embedding of CNTs. The Ti_3C_2Tx MXene was fabricated by the clay method. A Tyndall scattering effect can be seen in the colloid solution of exfoliated MXene nanosheets (Figure S1, Supporting Information), indicating their good dispersion. The carboxyl CNTs are chosen as the nanofillers because the carboxyl groups on the surface of CNTs and the hydroxyl groups on the surface of MXene can esterify to form ester groups, rather than simple physical mixing.[41] When the 1D CNTs are added into the 2D MXene solution, they are chemically interconnected on the MXene nanosheets through the esterification to form the chemical bridged MXene/CNT heterostructure. Therefore, the interlayer spacing of the MXene/CNT layered film is enlarged. Figure 1b,c gives transmission electron microscopy (TEM) images of the MXene/CNT at different magnifications, respectively, which clearly shows the heterostructure and the homogeneous embedding of CNTs on MXene nanosheets. The high-resolution TEM image of MXene/CNT (Figure 1d) also shows the interlinkage of CNTs in MXene nanosheets. The crystal lattice fringe with a spacing of 0.27 nm corresponds to the (100) lattice plane of MXene, while the lattice line with a spacing of 0.33 nm corresponds to the (002) plane of CNT. The cross-sectional SEM images of MXene/CNT film are shown in Figure 1e–f. It can be clearly seen that CNTs are embedded into the MXene nanosheets to form a well-connected 2D/1D layered structure compared to the pure MXene film (Figure S2, Supporting Information). It should be noted that embedding CNTs into the MXene layers can reduce the restacking of MXene nanosheets, improve the conductivity, and enhance the mechanical stability of the MXene layers. Meanwhile, the well-connected hierarchical heterostructure facilitates ion diffusion and accumulation. The main elements of MXene (Ti, C, O, and F) are also found to be evenly distributed on the section of the MXene/CNT film (Figure S3, Supporting Information), revealing the uniformity of the heterostructure. Figure S4 (Supporting Information) shows the Raman spectra of the MXene and MXene/CNT. The Raman peak at 202 cm^{-1} mainly corresponds to the out-of-plane stretching vibrations of Ti, C, and O atoms. The region 230–470 cm^{-1} represents in-plane vibrations of surface groups attached to titanium atoms, and the region between 580 and 730 cm^{-1} is assigned mostly to carbon vibrations.[42,43] The appeared peaks at 1355 and 1590 cm^{-1} in MXene/CNT are from the D and G bands of CNTs, confirming the existence of CNTs in heterostructures film.

In order to investigate the adjustment effect of intercalated CNT on the interlayer spacing of MXene film, the X-ray diffraction (XRD) patterns of MXene/CNT films with different MXene to CNT weight ratios are measured, as shown in Figure 1g. It can be seen that the characteristic diffraction peak corresponding to the (002) crystal plane of MXene in the pure MXene film is located at 6.8°. With the increase of the CNTs doping, the (002) diffraction peak in MXene/CNT film is correspondingly shifted to the left compared with the pure MXene film, indicating that the interlayer spacing of the stacked MXene nanosheets increases through the intercalation of CNTs. By adjusting the weight ratio of MXene to CNTs, the interlayer spacing of the MXene/CNT film can be controlled. By calculation, the interlayer spacing of pure MXene without CNT doping is ≈1.31 nm. When the MXene to CNT ratio increases to 1:2, the interlayer spacing of the MXene/CNT film increases to 1.42 nm, and the maximum adjusting interlayer spacing is 1.1Å (the inset of Figure 1g). Therefore, by controlling the chemical doping ratio of CNTs, the adjustment of the interlayer spacing of MXene films can be realized. Moreover, to confirm the esterification reaction between MXene and CNT, Fourier transform infrared (FTIR) spectra of the MXene, CNT, and MXene/CNT are measured, as shown in Figure S5 (Supporting Information). The typical characteristic peaks of MXene at ≈3456, 1637, and 544 cm^{-1} are the stretching vibration of —OH, C═O, and Ti—O, respectively.[44] For CNT, the bands at 1637 cm^{-1} and 1105 cm^{-1} are due to the carbonyl group (C═O), and C—O bond stretching of carboxylic acid groups, respectively.[45] It can be seen that the intensity of the hydroxyl is decreased in the MXene/CNT, which may be due to the transformation of the —OH to —COO bonds via the esterification reaction.[46] The most distinctive feature in the FTIR spectra of MXene/CNT are the bands at 1647, 1162, and 1110 cm^{-1}, which derive from the ester-bonded carbonyl group and the ester bond.[44,45,47] Therefore, the FTIR characterization indicates the covalent surface modification of MXene with CNT—COOH via the formation of the ester bond.

The mechanical property of MXene/CNTs film is also studied, as shown in Figure S6 (Supporting Information). It can be observed that the tensile strength and elongation at break values (32 MPa, 2.6%) of the MXene/CNT film are both enhanced compared with the MXene film without CNT doping (25 MPa, 0.4%), indicating the mechanical stability of CNT embedded in MXene and its advantage in the large deformation of the actuators. The conductivity of the MXene/CNT film is also measured (Figure S7, Supporting Information). Compared with pure MXene film (1070 S cm^{-1}), the MXene/CNT film exhibits a decreased electrical conductivity of 724 S cm^{-1}, due to the relatively low conductivity of the CNT. In addition, the pore size distribution of MXene and MXene/CNT films is also shown in Figure S8 (Supporting Information). Apparently, in comparison with the pure MXene film, micropores appear in MXene/CNT film, and the pore size distribution of MXene/CNT film becomes much more abundant. N2 adsorption/desorption isotherms (Figure S9, Supporting Information) further shows that MXene/CNT film possesses a larger specific surface area (166.53 m^2g^{-1}) than that of the pure MXene film (35.19 m^2g^{-1}), permitting more accessible ions in the electrode. The well-interconnected porous structured MXene/CNT film with more abundant micro and mesopores and larger specific surface area is highly beneficial to the improvement of ion storage and fast diffusion in the electrodes, which promotes to enhance the response speed and volume change of the ionic actuators.

2.2. Electrochemical Characterization

To evaluate the energy-storage value of the MXene/CNT, a flexible ionic actuator is constructed by laminating two pieces of MXene/CNT heterostructure composite films with a solid electrolyte layer containing thermoplastic polyurethane (TPU) integrated with ionic liquid ($EMIBF_4$), which is schematically shown in **Figure 2a**. The cross-sectional SEM image of this MXene/CNT actuator (inset of Figure 2a) clearly shows the three-layer sandwiched structure of the actuator. A strong interlayer adhesion between the MXene/CNT electrode and the polyelectrolyte layer is also observed, which is favorable for ion diffusion and deformation stability. Furthermore, as the MXene/CNT actuators are prepared by hot pressing, the oxidation of MXene in the MXene/CNT electrode before and after hot pressing is further investigated through X-ray photoelectron spectroscopy (XPS) testing. As shown in the Ti 2p spectra in Figure S10 (Supporting Information), the MXene before hot pressing exhibits the characteristic peaks located at 455.5, 456.3, 457.6, and 459.5 eV, which correspond to the Ti $2p_{3/2}$ electron orbital of the Ti—C bond, Ti (II), Ti (III) and Ti—O bond, respectively. The characteristic peak of the binding energy above 460 eV is the corresponding peak of the electron orbital of Ti $2p_{1/2}$. After hot pressing, the strength of the Ti—C bond in MXene decreases, while the strength of the Ti–O bond increases (Table S1, Supporting Information). These results indicate the surface functional groups of MXene are changed and the direct covalent interaction between Ti and C is reduced. It is worth noting that although hot pressing causes a certain degree of oxidation, the oxidation of the MXene is maintained as a mild surface phenomenon.[48,49] This is because the esterification and hydrogen bonding between the oxygen-containing functional groups on the surface of CNT and MXene partially limit the oxidation of Ti. Therefore, hot pressing treatment may not cause severe oxidation on the surface of MXene,[48] and will not have a significant impact on its actuation performance.

In order to study the ion kinetic diffusion and storage in the MXene/CNT actuators, the electrochemical impedance spectroscopy (EIS) measurement is performed, as shown in Figure 2b. Here the weight ratio of Mxene to CNT is 1:1. It can be seen that the Nyquist plots include a depressed semicircle in the high-frequency region, a Warburg diffusion in the medium-frequency region, and an intercalation capacitance in the

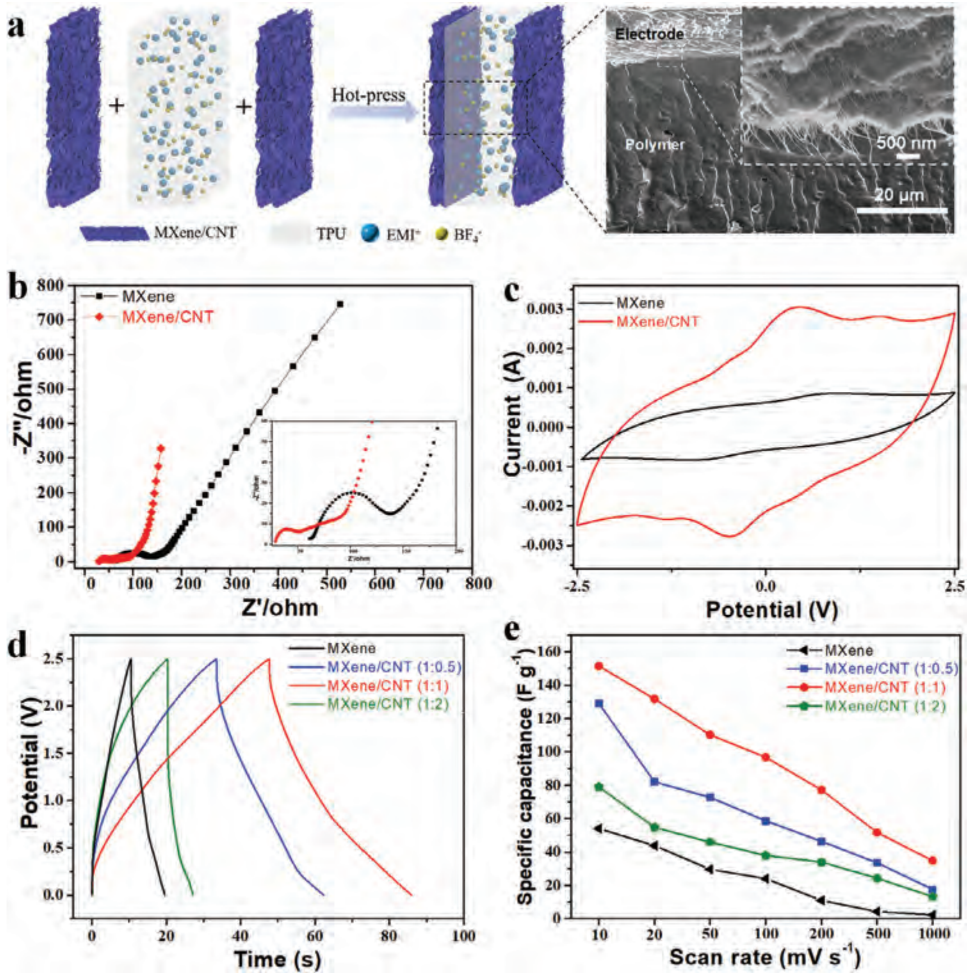

Figure 2. Assembly and electrochemical performance of the MXene/CNT actuator. a) Schematic diagram of the fabrication process of the MXene/CNT actuator. The inset shows a cross-sectional SEM image of the actuator. b) Nyquist plots of the actuators. The inset is the depressed semicircle of Nyquist plots. c) CV curves of the MXene and MXene/CNT actuators at a scan rate of 100 mV s^{-1}. d) Galvanostatic charge/discharge curves of the MXene and MXene/CNT actuators at a current density of 1 A g^{-1}. e) The calculated specific capacitance performance of the MXene/CNT and MXene actuators under different scan rates.

low-frequency region.[20] The equivalent circuit model is also shown in Figure S11 (Supporting Information). It includes the following parameter values: R0 represents the inner resistance of the actuator; Q_1/R_1 is the contact impedance, reflecting the electron conduction from the metal electrode to the actuator electrode; Z_w is the diffusion impedance, indicating the ion diffusion ability in the actuator; C_1 is the intercalation capacitance, indicating that the ion accumulates in electrode interfaces. Compared with the pure MXene-based actuator, the MXene/CNT actuator shows better electrical contact, ion diffusion capability, and energy storage capability, which is beneficial for the electrochemical actuation.

The cyclic voltammogram (CV) curves of the MXene/CNT actuators are also performed to estimate the electrochemical performance. In this test, all measurements were carried out in TPU/$EMIBF_4$ polyelectrolyte under the applied voltage from −2.5 V to + 2.5 V and a scanning rate of 10 to 1000 mV s^{-1}. As shown in Figure 2c, the MXene/CNT actuator (weight ratio of 1:1) shows a significant improvement in the CV curve area compared with the MXene actuator, indicating an increase in the electrochemical energy storage. The redox peaks in the CV curve may arise from a Faradaic process in MXene, which can act as active sites to enhance charge storage through pseudo-capacitance.[36,50] In addition, the galvanostatic charge–discharge test (Figure 2d) is measured at a current density of 1A g-1 to further evaluate the energy storage performance of the actuators. Here the MXene/CNT actuators with different weight ratios of MXene to CNT are also employed in the test. Compared to the actuators with different weight ratios, the MXene/CNT actuator with a weight ratio of 1:1 shows the highest charge/discharge capability with a symmetrical triangular shape, which indicates good reversibility and coulombic efficiency.

The specific capacitance of the MXene/CNT actuators with different weight ratios is also calculated, as shown in Figure 2e. MXene/CNT-based actuator with a 1:1 weight ratio has a specific capacitance of 151.5 F g^{-1} which is larger than that of the pure MXene actuator (54.03 F g^{-1}) and the MXene/CNT actuators with other weight ratio at a scan rate of 10 mV s^{-1}. When

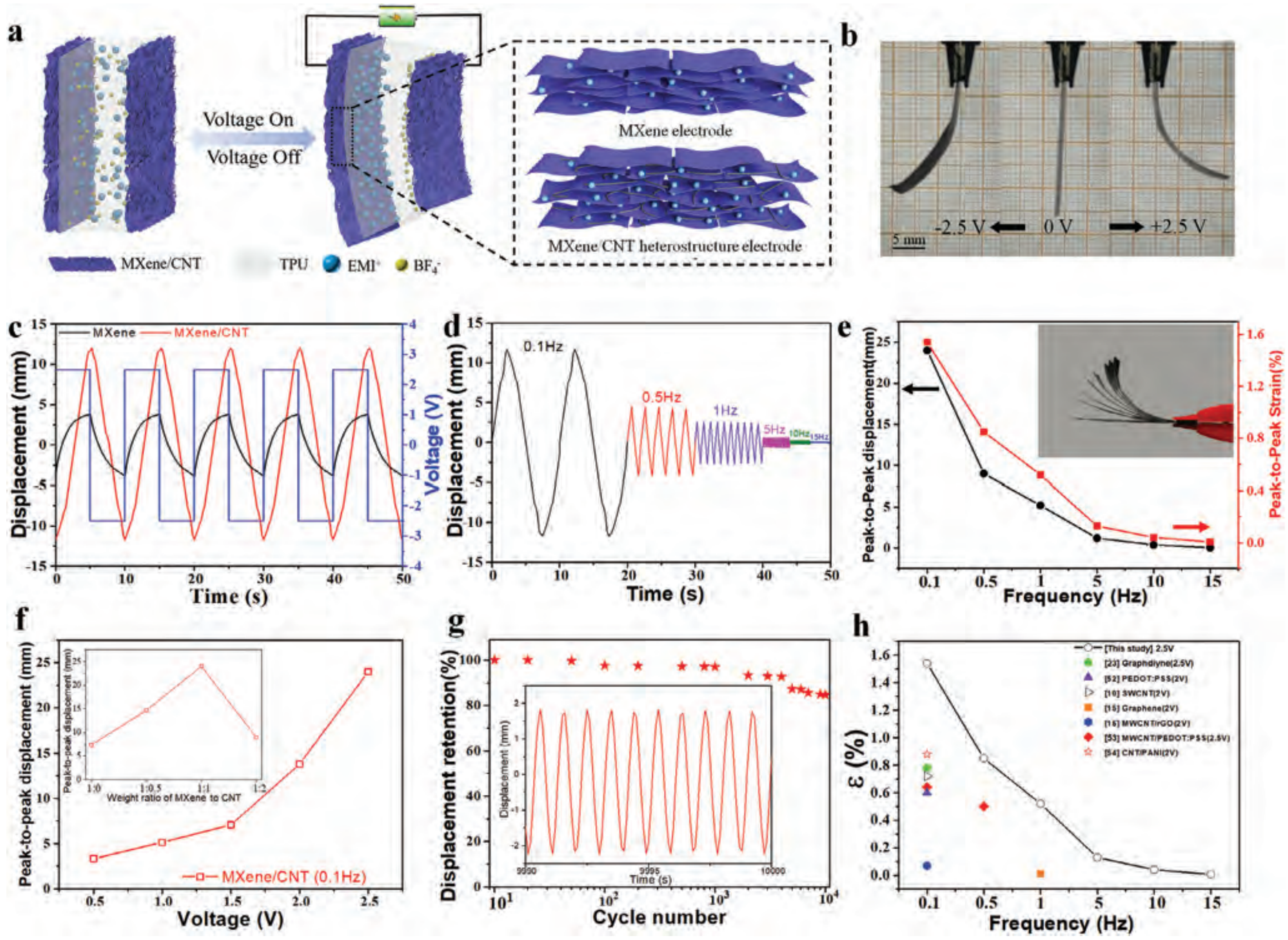

Figure 3. Actuation performance of the MXene/CNT actuators. a) Schematic diagram of the actuation mechanism of the MXene/CNT actuator. b) Optical images of the reversible bending deformation of the MXene/CNT actuator under ±2.5 V 0.1 Hz voltage. c) Bending deformation displacement of the actuators under ±2.5 V 0.1 Hz voltage. d) Actuation displacements of the MXene/CNT actuator with different voltage frequencies. e) Peak-to-peak displacement and strain of the MXene/CNT actuator under ±2.5 V voltage with different frequencies. The inset shows an optical image of the actuator under 2.5 V voltage for 15s. f) Peak-to-peak displacement of the actuator under 0.1 Hz voltage with different amplitude. The inset shows the peak-to-peak displacement of the actuator under voltage with different MXene to CNT weight ratios. g) Cyclic actuation stability of the MXene/CNT actuator. The inset shows the detailed displacement during actuation cycles. h) Comparison of the deformation strain of the MXene/CNT actuator with other reported ionic electrochemical actuators at different frequencies.

the scat rate increases from 10 to 1000 mV s^{-1}, the MXene/CNT actuator with 1:1 ratio also exhibits a larger specific capacitance value than the actuators with another weight ratio, which mainly is attributed to the porous layered heterostructure with adjusted interlayer spacing, high electrical conductivity and electrochemical activity that provide accessible ionic pathways for the fast ion transport and storage. However, when the weight ratio of MXene to CNT increases to 1:2 in the electrode, the specific capacitance of the MXene/CNT actuator is reduced. As we know, MXene has good electrical and electrochemical properties. The embedment of CNTs in MXene layers also leads to the increase of the interlayer spacing and specific surface area. However, once the amount of CNTs embedded in MXene is too much, it would impair the 2D layered network structure formed by MXene and CNT as well as the good capacitance characteristics of the MXene, leading to the decrease of the whole electrochemical performance.

2.3. Electrochemical Actuation

The excellent electrochemical performance of the MXene/CNT actuator enables it to excel in ionic electrochemical actuators. **Figure 3a** shows the schematic diagram of the actuation mechanism of the MXene/CNT actuator. When an electrical voltage is applied to the actuator, the movable anion and cation in the polymer electrolyte layer move to the opposite electrodes on both sides through the electrode/electrolyte interface driven by the electric field, resulting in the volume change of the electrodes. Due to the diameter difference between the cation EMI^+ (0.606 nm) and anion BF_4^- (0.454 nm), the cathode expands, and the anode contracts, leading to the bending deformation of the whole actuator toward the anode side. The inset of Figure 3a also provides the difference between the mobile ions that enter the MXene electrode and the MXene/CNT electrode after applying electrical voltage. Compared with the

MXene actuator, the MXene/CNT actuator has better electrochemical actuation performance, which is mainly attributed to the following aspects. First, as a 1D nanostructured material, CNT can be uniformly inserted between the 2D MXene layers. The CNT embedment enlarges the interlayer spacing of MXene layers and alleviates the restacking of MXene nanosheets, which can increase the specific surface area, improve the ion storage capacity of the electrode layer, and increase the deformation displacement of the actuator. Second, the enlarged interlayer spacing also enhances the ion channels, which would accelerate the ion migration rate and shorten the response time of the actuator. In addition, compared with the MXene actuator with poor flexibility and weak adhesion between the MXene electrode and electrolyte layer that leads to flaking and delamination of electrode material (Figure S12a, Supporting Information), the flexibility, adhesion between layers, and mechanical durability of the MXene/CNT actuator are significantly improved after the good interconnection of CNTs inside the layered MXene nanosheets. As shown in Figure S12b (Supporting Information), no flaking of the electrode or delamination is observed in the MXene/CNT actuator, which facilitates the large actuation performance. Figure 3b shows the optical images of the electrochemical actuation of the MXene/CNT actuator. Here, if not mentioned, the following weight ratio of MXene to CNT in the MXene/CNT actuators is all 1:1. After applying electrical voltage in different directions (±2.5 V, 0.1 Hz), the actuator bends in the corresponding different directions. A video of the electrochemical actuation of the MXene/CNT actuator under 0.1 Hz 2.5 V voltage is also provided in Movie S1 (Supporting Information).

The generated detailed displacement of the MXene/CNT actuators under 0.1 Hz square wave voltage (±2.5 V) is also shown in Figure 3c. The displacement of the MXene actuator under the same voltage is also provided for comparison. It is clearly seen that the MXene/CNT actuator exhibits large bending deformation with a peak-to-peak displacement of 24 mm which is ≈3 times higher than that of the MXene actuator. By calculation, this peak-to-peak deformation strain of the MXene/CNT actuator under ±2.5 V, 0.1 Hz can reach up to 1.54%, which is larger than the peak-to-peak strain of the MXene actuator. This is attributed to the fact that by constructing MXene/CNT heterostructured electrodes with adjustable interlayer spacing, there will be more charge storage and ion channels in the electrode, which can produce larger deformation. In comparison, the bending displacement of the MXene actuator is relatively small, which is mainly due to the restacking of MXene nanosheets for limiting the ion intercalation and the poor mechanical flexibility of the MXene electrode. By changing the frequency of the applied voltage, the displacement of the actuator can be further controlled. Figure 3d shows the displacement of the MXene/CNT actuator under ±2.5 V voltage with different frequencies. With the increase of the voltage frequency, the bending displacement decreases accordingly. Under the 15 Hz voltage stimulation, the actuator still produces a corresponding mechanical response with the same frequency, while the pure MXene actuator almost loses the frequency response at 15 Hz. The detailed peak-to-peak displacement and strain of the MXene/CNT actuator under different frequencies (0.1–15 Hz) are also provided in Figure 3e. The displacement decreases with the increase of voltage frequency, which is mainly due to the fact that ions need a certain response time to migrate under electric field stimulation. At higher voltage frequencies, the ions far from the electrode layer do not have enough time to migrate into the electrode layer in time to produce effective bending deformation. When the voltage frequency is <0.1 Hz, the actuator can produce larger bending deformation. The inset image in Figure 3e shows the deformation of the MXene/CNT actuator under the continuous 2.5 V voltage stimulation for 15 s. With the increase of the stimulation time, the actuator continues to bend upward. The relationship between the generated displacement of the MXene/CNT actuator and its driving voltage is also studied (Figure 3f). With the increase of voltage, the deformation displacement increases correspondingly. In addition, the bending displacement varies with the doping amount of CNT in the MXene/CNT electrode (the inset of Figure 3f). After applying 2.5 V voltage for 5 s, the MXene/CNT actuator with a 1:1 weight ratio of MXene to CNT shows the optimal displacement. This is consistent with its excellent electrochemical performance. Furthermore, the unidirectional deformation displacement of MXene/CNT actuators with different weight ratios under 0.1 Hz 2.5 V voltage is also provided in Figure S13 (Supporting Information). The MXene/CNT actuator with a weight ratio of 1:1 shows the highest deformation displacement. The long-term operation stability of this actuator under continuous square wave electrical voltage stimulation is also evaluated, as shown in Figure 3g. After ≈10 000 cycles of continuous deformation, the MXene/CNT actuator still exhibits good cyclic stability. The slight displacement degradation may be due to a small amount of evaporation of ionic liquid in the air, as well as the fact that some of the ions remaining in the electrode layer during repeated cycling do not return to the middle layer in time, which results in the reduction of the total amount of the mobile ions.[20]

Besides the excellent deformation performance, the actuator also exhibits excellent mechanical output force. It can move a clip with a weight of 500 mg (15 times its own weight) under 2.5 V voltage stimulation (Figure S14 and Movie S2, Supporting Information). The detailed blocking force output under different electrical voltages is also shown in Figure S15 (Supporting Information). The actuator can generate ≈5 mN force output under 2.5 V voltage, which is larger than that of the reported nanocarbon or MXene electrode-based ionic actuators.[7,15,17,18,32,51] We also compare the actuation performance of the MXene/CNT actuator with other electrode material-based ionic actuators at different frequencies, as shown in Figure 3h[10,15,23,52–54] and Table S2 (Supporting Information). The MXene/CNT actuator produces a peak-to-peak deformation strain of 1.54% at 0.1 Hz 2.5 V voltage. When the frequency increases to 1 Hz, it still maintains a good strain of 0.52%. In comparison with the ionic electrochemical actuators based on other electrode materials, the MXene/CNT-based actuator shows excellent deformation performance.

2.4. Biomimetic Applications

Due to the ion migration mechanism similar to supercapacitors, the ionic actuators have charged ions on their surface, which can mimic the human fingers to touch capacitive screens on smart devices such as smartphones and tablets. By utilizing the large deformation, variable frequency, and high stability of this MXene/CNT actuator, it is expected to achieve human-computer

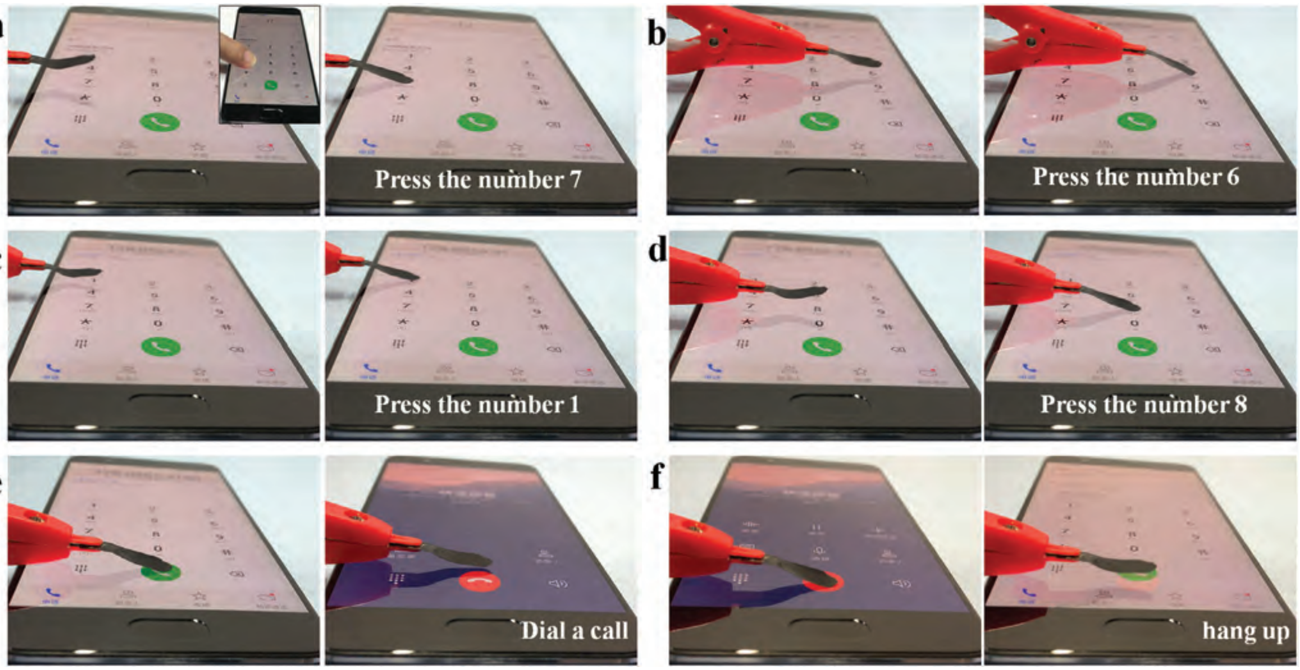

Figure 4. An artificial finger based on the MXene/CNT actuator mimics the human finger to press numbers on a smartphone to dial a call (a–e) and hang up the call (g) under the electrical stimulation. The inset image of (a) is the human finger's pressing number for comparison.

interaction touch manipulation similar to or even beyond human fingers on smart devices. As shown in **Figure** 4 and Movie S3 (Supporting Information), the MXene/CNT actuator can act as an artificial finger that mimics the human finger (inset in Figure 4a) to press the phone numbers on the smartphone to make a call under the electrical voltage stimulation (1 Hz 2.5 V). Moreover, an electronic drum APP is used to further show the touching manipulation of the actuator on the smartphone. As given in **Figure** 5a, the MXene/CNT actuator can serve as the artificial finger to perform flexible tapping with variable frequency on the drum APP in the smartphone, and its tapping frequency can be changed by controlling the frequency of the driven voltage. Figure 5b,c (Movies S4 and S5, Supporting Information) give the optical images of the actuator tapping the drum APP in a smartphone under 2.5 V voltage stimulation at 1 and 10 Hz, respectively. It can be seen that the vibration frequency produced by tapping the drum is consistent with the frequency of the applied driving voltage. Furthermore, the artificial finger based on this actuator is designed to achieve high-frequency tapping of up to 13 Hz on the drum (Figure 5d; Movie S6, Supporting Information). This frequency can even exceed the normal tapping frequency of the human finger (7.5 Hz) on a smartphone (Figure 5e; Movie S7, Supporting Information). Besides the single-finger manipulation, we also use two artificial fingers to achieve synergistic sequential tapping on the drum App (Figure 5f; Movie S8, Supporting Information). This indicates that the MXene/CNT actuators can be designed to perform more complex coordinated human-computer interaction touch manipulation tasks on smart touchscreen devices.

Moreover, the other biomimetic applications of this MXene/CNT actuator are also explored. First, because the actuator has excellent mechanical output, it can be assembled into a flexible artificial claw for manipulating objects. As shown in **Figure** 6a and the Movie S9 (Supporting Information), upon 2.5 V electrical voltage stimulation, the artificial claw made of four pieces of actuators can grasp, move, and put down an object (150 mg) whose weight is 6 times more than its own weight within 6 s. In addition, taking advantage of the large deformation and easy cutting features of the actuator, a biomimetic dragonfly-like robot is prepared by cutting the actuators into the shape of the dragonfly wings. After applying 2.5 V electrical voltage, the robot can simulate the wings flapping movement of the dragonfly (Figure 6b; Movie S10, Supporting Information). The MXene/CNT actuator can be also driven by light irradiation once combined with solar cells. As shown in Figure 6c, the actuator is connected to a solar panel. The actuator remains unchanged without light irradiation. Once exposed to light irradiation, it produces a bending deformation. When further cutting the actuators into leaf shapes, the opening and closing behaviors of the artificial leaves with or without light are realized (Figure 6d; Movie S10, Supporting Information).

3. Conclusion

We have developed an electrochemical ionic actuator based on MXene/CNT heterostructure electrodes with large deformation, wide frequency response, and high actuation stability, and achieved its human-computer interaction applications. This heterostructure electrode utilizes the excellent conductivity and 2D layered structure of MXene nanosheets, as well as the doping of 1D CNT for adjusting the interlayer spacing of MXene layers. The increase in interlayer spacing in layered MXene film is beneficial for ion migration and storage. Meanwhile, the

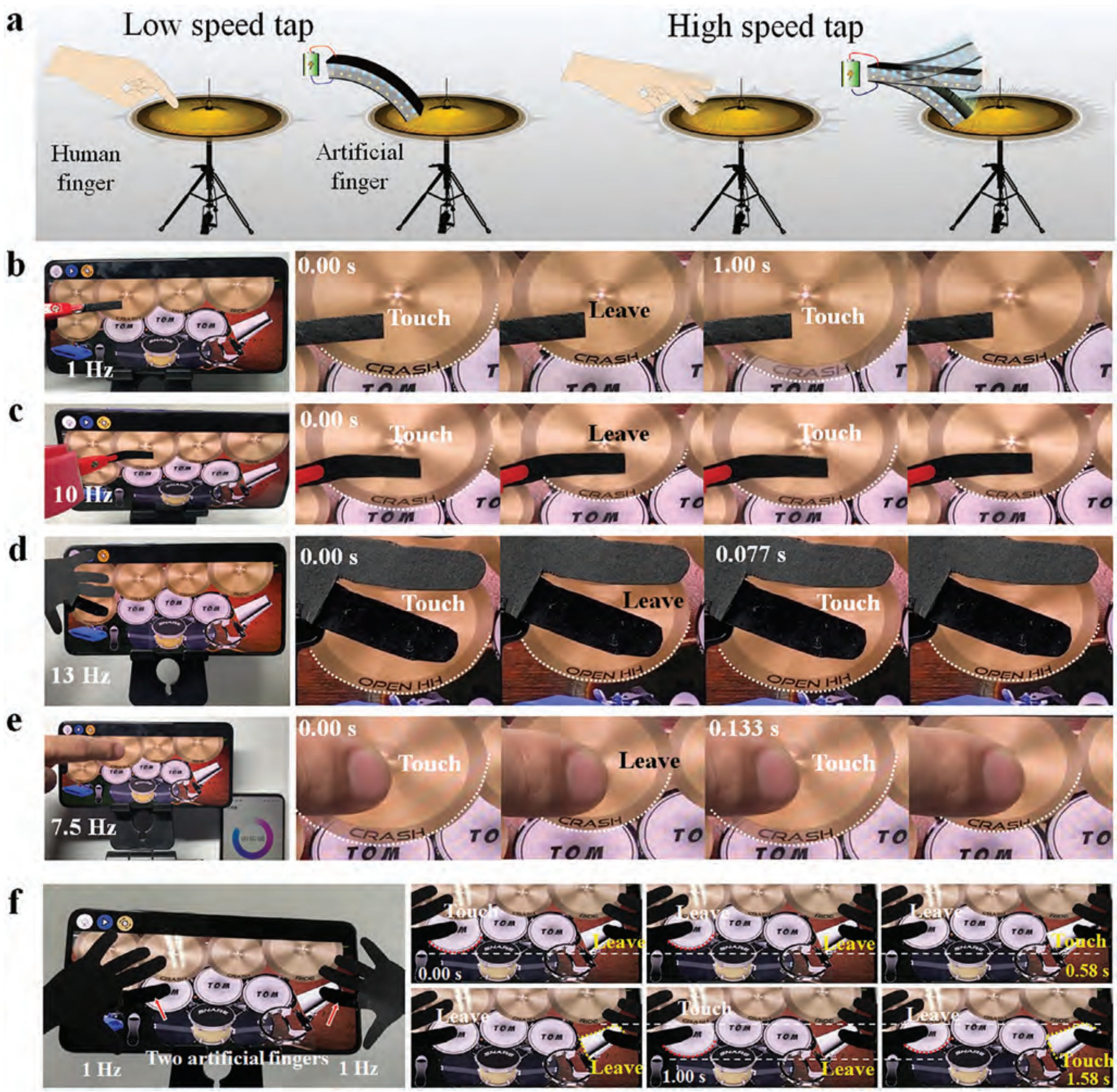

Figure 5. MXene/CNT actuators as soft artificial fingers to play drums on a smartphone with tunable frequency. a). Schematic diagram of the drum beating by a human finger and an artificial finger at low and high tapping speeds. b,c) Optical images showing the MXene/CNT actuator put above the smartphone to tap the drum at different frequencies of 1 and 10 Hz. d) An artificial finger based on the MXene/CNT actuator for tapping the drum with a frequency of 13 Hz. e) A human finger-tapping the drum on the smartphone with a frequency of ≈7.5 Hz for comparison. f) Two artificial fingers based on MXene/CNT actuators are driven by 1 Hz 2.5 V voltage to tap different drums in turn on the smartphone.

addition of CNT also improves the mechanical stability of MXene electrodes. Therefore, MXene/CNT electrode greatly promotes the deformation behavior caused by electrical field-driven ion migration. Under 2.5 V voltage stimulation, the actuator using this MXene/CNT heterostructures as electrodes shows low electrical voltage driven high actuation performance, including large peak-to-peak bending deformation (displacement of 24 mm, strain of 1.54%), controllable wide frequency response (0.1–15 Hz), high power density (18.44 kW m^{-3}) and energy density (7.04 kJ m^{-3}), as well as excellent cycling stability (10 000 cycles). It can also move a clip with a weight of 500 mg (15 times its own weight) under 2.5 V voltage stimulation. Besides, after connecting to a solar panel, the MXene/CNT actuator can even bend under light illumination. Based on its excellent deformation performance, this actuator can be applied as an artificial finger in human-computer interaction, for pressing the phone number to make a call on a

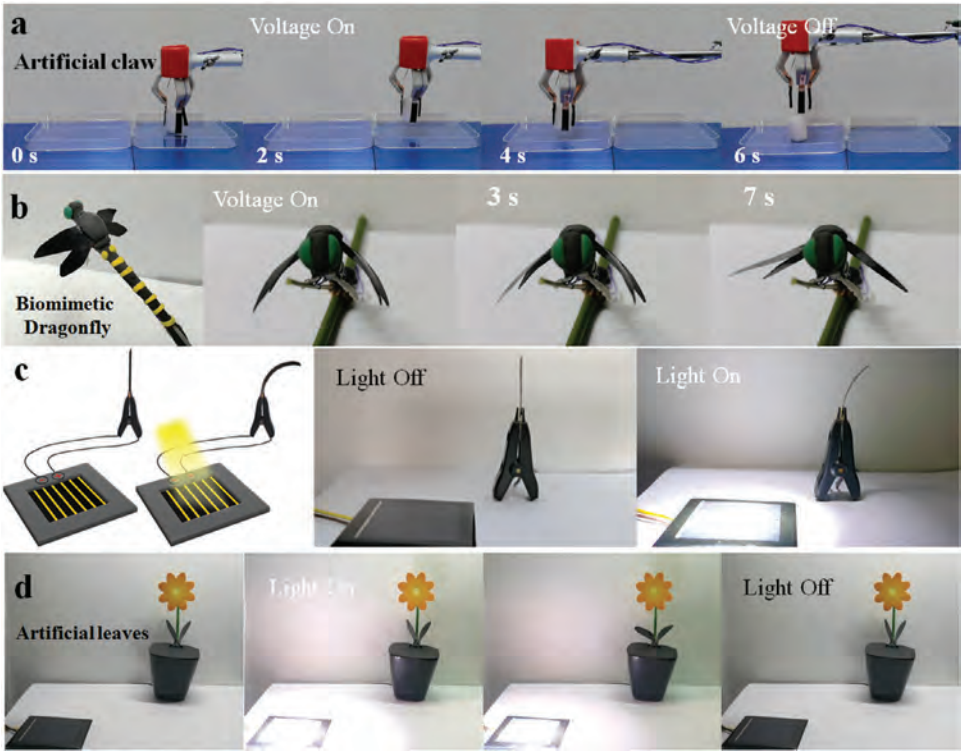

Figure 6. Biomimetic applications of the MXene/CNT actuators. a) An artificial claw based on the actuators for grasping objects under electrical voltage stimulation. b) A biomimetic dragonfly mimics the wing flapping movement. c) The actuator is connected to a solar panel to realize bending deformation light irradiation. d) Artificial leaves based on the actuators to open and close under light irradiation.

smartphone, and for tapping on a drum APP at a high speed of 13 Hz, which is even higher than the tapping frequency that a normal person can reach. We also explored other biomimetic applications of the actuator, including flexible artificial claws that can grasp objects that are 6 times their own weight, biomimetic dragonfly that flaps their wings, and artificial leaves that open under light. These results reveal the importance of 2D/1D heterostructure electrodes in ionic actuators and provide the foundation for their practical applications in the fields of human-computer interaction and biomimetic robots.

Supporting Information

Supporting Information is available from the Wiley Online Library or from the author.

Acknowledgements

This work was supported by the National Natural Science Foundation of China (2227504822275048, 22411530048), the Fundamental Research Funds for the Central Universities of China (JZ2023YQTD0074), the Anhui Provincial Natural Science Foundation (2008085J22), and Funding from the Technology Area Fund of the Basic Strengthening Program (2021-JCJQ-JJ-0026).

Conflict of Interest

The authors declare no conflict of interest.

Data Availability Statement

The data that support the findings of this study are available from the corresponding author upon reasonable request.

Keywords

biomimetic devices, electrochemical actuators, human-computer interaction, MXene, soft robots

Received: May 17, 2024
Revised: June 25, 2024
Published online: July 11, 2024

[1] A. Prindle, J. Liu, M. Asally, S. Ly, J. Garcia-Ojalvo, G. M. Suel, *Nature* **2015**, *527*, 59.
[2] C. Paulino, V. Kalienkova, A. K. M. Lam, Y. Neldner, R. Dutzler, *Nature* **2017**, *552*, 421.
[3] S. Liu, Y. Liu, H. Cebeci, R. Villoria, J. Lin, B. L. Wardle, Q. M. Zhang, *Adv. Funct. Mater.* **2010**, *20*, 3266.
[4] Y. Shi, Y. Wu, S. Wang, Y. Zhao, T. Li, X. Yang, T. Zhang, *J. Am. Chem. Soc.* **2021**, *143*, 4017.
[5] X. Zhu, Y. Hu, G. Wu, W. Chen, N. Bao, *ACS Nano* **2021**, *15*, 9273.
[6] M. Mahato, R. Tabassian, V. H. Nguyen, S. Oh, S. Nam, W. J. Hwang, I. K. Oh, *Nat. Commun.* **2020**, *11*, 5358.
[7] L. Liu, C. Wang, Z. Wu, Y. Xing, *ACS Appl. Mater. Interfaces* **2022**, *14*, 18150.

[8] F. Wang, Q. Li, J. O. Park, S. Zheng, E. Choi, *Adv. Funct. Mater.* **2021**, *31*, 2007749.
[9] L. Chang, Y. Liu, Q. Yang, L. Yu, J. Liu, Z. Zhu, P. Lu, Y. Wu, Y. Hu, *J. Bionic. Eng.* **2018**, *15*, 765.
[10] T. Sugino, K. Kiyohara, I. Takeuchi, K. Mukai, K. Asaka, *Sens. Actuators, B* **2009**, *141*, 179.
[11] L. Lu, J. Liu, Y. Hu, Y. Zhang, W. Chen, *Adv. Mater.* **2013**, *25*, 1270.
[12] G. Wu, Y. Hu, W. Chen, *Chin. Sci. Bull.* **2014**, *59*, 2240.
[13] G. Wu, Y. Hu, J. Zhao, T. Lan, D. Wang, Y. Liu, W. Chen, *Small* **2016**, *12*, 4986.
[14] G. Wu, G. Li, T. Lan, Y. Hu, Q. Li, T. Zhang, W. Chen, *J. Mater. Chem. A* **2014**, *2*, 16836.
[15] L. Lu, J. Liu, Y. Hu, Y. Zhang, H. Randriamahazaka, W. Chen, *Adv. Mater.* **2012**, *24*, 4317.
[16] M. Kotal, R. Tabassian, S. Roy, S. Oh, I. K. Oh, *Adv. Funct. Mater.* **2020**, *30*, 1910326.
[17] M. Kotal, J. Kim, K. J. Kim, I. K. Oh, *Adv. Mater.* **2016**, *28*, 1610.
[18] G. Wu, Y. Hu, Y. Liu, J. Zhao, X. Chen, V. Whoehling, C. Plesse, G. T. M. Nguyen, F. Vidal, W. Chen, *Nat. Commun.* **2015**, *6*, 7258.
[19] M. Kotal, J. Kim, R. Tabassian, S. Roy, V. H. Nguyen, N. Koratkar, I. K. Oh, *Adv. Funct. Mater.* **2018**, *28*, 1802464.
[20] G. Wu, X. Wu, Y. Xu, H. Cheng, J. Meng, Q. Yu, X. Shi, K. Zhang, W. Chen, S. Chen, *Adv. Mater.* **2019**, *31*, 1806492.
[21] M. Acerce, E. K. Akdoğan, M. Chhowalla, *Nature* **2017**, *549*, 370.
[22] M. T. Manzoor, V. H. Nguyen, S. Umrao, J. H. Kim, R. Tabassian, J. E. Kim, I. K. Oh, *Adv. Funct. Mater.* **2019**, *29*, 1905454.
[23] C. Lu, Y. Yang, J. Wang, R. Fu, X. Zhao, L. Zhao, Y. Ming, Y. Hu, H. Lin, X. Tao, Y. Li, W. Chen, *Nat. Commun.* **2018**, *9*, 752.
[24] S. Roy, J. Kim, M. Kotal, R. Tabassian, K. J. Kim, I. K. Oh, *Adv. Funct. Mater.* **2019**, *29*, 1900161.
[25] B. Anasori, Y. Gogotsi, *2D Metal Carbides and Nitrides (MXenes)*, 1st ed., Springer, Berlin **2019**.
[26] M. Naguib, M. Kurtoglu, V. Presser, J. Lu, J. Niu, M. Heon, L. Hultman, Y. Gogotsi, M. W. Barsoum, *Adv. Mater.* **2011**, *23*, 4248.
[27] J. L. Hart, K. Hantanasirisakul, A. C. Lang, B. Anasori, D. Pinto, Y. Pivak, J. T. van Omme, S. J. May, Y. Gogotsi, M. L. Taheri, *Nat. Commun.* **2019**, *10*, 522.
[28] A. Lipatov, H. Lu, M. Alhabeb, B. Anasori, A. Gruverman, Y. Gogotsi, A. Sinitskii, *Sci. Adv.* **2018**, *4*, eaat0491.
[29] M. Ghidiu, M. R. Lukatskaya, M. Q. Zhao, Y. Gogotsi, M. W. Barsoum, *Nature* **2014**, *516*, 78.
[30] M. Acerce, D. Voiry, M. Chhowalla, *Nat. Nanotechnol.* **2015**, *10*, 313.
[31] J. Come, J. M. Black, M. R. Lukatskaya, M. Naguib, M. Beidaghi, A. J. Rondinone, S. V. Kalinin, D. J. Wesolowski, Y. Gogotsi, N. Balke, *Nat. Energy* **2015**, *17*, 27.
[32] D. Pang, M. Alhabeb, X. Mu, Y. Dall'Agnese, Y. Gogotsi, Y. Gao, *Nano Lett.* **2019**, *19*, 7443.
[33] S. Umrao, R. Tabassian, J. Kim, V. H. Nguyen, Q. Zhou, S. Nam, I. K. Oh, *Sci. Rob.* **2019**, *4*, eaaw7797.
[34] M. Q. Zhao, X. Xie, C. E. Ren, T. Makaryan, B. Anasori, G. Wang, Y. Gogotsi, *Adv. Mater.* **2017**, *29*, 1702410.
[35] L. Xiu, Z. Wang, M. Yu, X. Wu, J. Qiu, *ACS Nano* **2018**, *12*, 8017.
[36] Z. Pan, L. Kang, T. Li, M. Waqar, J. Yang, Q. Gu, X. Liu, Z. Kou, Z. Wang, L. Zheng, J. Wang, *ACS Nano* **2021**, *15*, 12975.
[37] Q. Wang, X. Pan, C. Lin, H. Gao, S. Cao, Y. Ni, X. Ma, *Chem. Eng. J.* **2020**, *401*, 126129.
[38] T. Wang, T. Wang, C. Weng, L. Liu, J. Zhao, Z. Zhang, *Nano Res.* **2021**, *14*, 2277.
[39] S. Chen, J. H. Ciou, F. Yu, J. Chen, J. Lv, P. S. Lee, *Adv. Mater.* **2022**, *34*, 2200660.
[40] M. Garai, M. Mahato, S. Nam, E. Kim, D. Seo, Y. Lee, V. H. Nguyen, S. Oh, P. Sambyal, H. Yoo, A. K. Taseer, S. A. Syed, H. Han, C. W. Ahn, J. Kim, I. K. Oh, *Adv. Funct. Mater.* **2023**, *33*, 2212252.
[41] Q. Li, H. Cheng, X. Wu, C. Wang, G. Wu, S. Chen, *J. Mater. Chem. A* **2018**, *6*, 14112.
[42] T. Hu, J. Wang, H. Zhang, Z. Li, M. Hu, X. Wang, *Phys. Chem. Chem. Phys.* **2015**, *17*, 9997.
[43] A. Sarycheva, Y. Gogotsi, *Chem. Mater.* **2020**, *32*, 3480.
[44] Q. Guo, X. Zhang, F. Zhao, Q. Song, G. Su, Y. Tan, Q. Tao, T. Zhou, Y. Yu, Z. Zhou, C. Lu, *ACS Nano* **2020**, *14*, 2788.
[45] W. T. Xu, Z. Xu, Y. X. Liang, L. M. Liu, W. Weng, *Nanotechnology* **2021**, *32*, 355706.
[46] J. T. Lee, B. C. Wyatt, G. A. Davis Jr., A. N. Masterson, A. L. Pagan, A. Shah, B. Anasori, R. Sardar, *ACS Nano* **2021**, *15*, 19600.
[47] K. M. Zhang, J. W. Sun, J. Y. Song, C. H. Gao, Z. Wang, C. X. Song, Y. M. Wu, Y. T. Liu, *ACS Appl. Mater. Interfaces* **2020**, *12*, 45306.
[48] H. Li, R. Chen, M. Ali, H. Lee, M. J. Ko, *Adv. Funct. Mater.* **2020**, *30*, 2002739.
[49] C. Wang, R. Cheng, P.-X. Hou, Y. Ma, A. Majeed, X. Wang, C. Liu, *ACS Appl. Mater. Interfaces* **2020**, *12*, 43032.
[50] M. R. Lukatskaya, S. Kota, Z. Lin, M. Zhao, N. Shpigel, M. D. Levi, J. Halim, P. L. Taberna, M. W. Barsoum, P. Simon, Y. Gogotsi, *Nat. Energy* **2017**, *2*, 17105;
[51] O. Kim, H. Kim, U. H. Choi, M. J. Park, *Nat. Commun.* **2016**, *7*, 13576.
[52] S. Y. Kim, Y. Kim, C. Cho, H. Choi, H. W. Park, D. Lee, E. Heo, S. Park, H. Lee, D. H. Kim, *ACS Appl. Mater. Interfaces* **2019**, *11*, 29350.
[53] D. Wang, C. Lu, J. Zhao, S. Han, M. Wu, W. Chen, *RSC Adv.* **2017**, *7*, 31264.
[54] T. Sugino, K. Kiyohara, I. Takeuchi, K. Mukai, K. Asaka, *Carbon* **2011**, *49*, 3560.